

2 Interacting Fermion Systems: Hubbard-Stratonovich Trick

So far we have dealt with free quantum fields in the absence of interactions and have obtained nice closed expressions for the thermodynamic potential, i.e., therefore also for the generating functionals of the thermodynamic Green functions. However, once we switch on the interactions in our model field theories, there is only a very limited class of soluble models, in general we have to apply approximations. The most common technique is based on perturbation theory, which requires a small parameter. For strong interactions at low momentum transfer (the infrared region), the coupling is nonperturbatively strong and alternative, nonperturbative methods have to be invoked. One of the strategies, which is especially suitable for the treatment of quantum field theories within the path integral formulation is based on the introduction of collective variables (auxiliary fields) by an exact integral transformation due to Stratonovich and Hubbard which allows to eliminate (integrate out) the elementary degrees of freedom. Generally, the (dual) coupling of the auxiliary fields is weak so that perturbative expansions of the nonlinear effective action make sense and provide useful results already at low orders of this expansion.

A general class of interactions for which the Hubbard-Stratonovich (HS) transformation is immediately applicable, are four-fermion couplings of the current-current type

$$\mathcal{L}_{int} = G(\bar{\psi}\psi)^2 . \quad (87)$$

A Fermi gas with this type of interaction serves as a model for electronic superconductivity (Bardeen-Cooper-Schrieffer (BCS) model, 1957) or for chiral symmetry breaking in quark matter (Nambu–Jona-Lasinio (NJL) model, 1961).

The HS-transformation for (87) reads

$$\exp \left[G(\bar{\psi}\psi)^2 \right] = \mathcal{N} \int \mathcal{D}\sigma \exp \left[\frac{\sigma^2}{4G} + \bar{\psi}\psi\sigma \right] \quad (88)$$

and allows to bring the functional integral over fermionic fields into a quadratic (Gaussian) form so that fermions can be integrated out. This is also called *Bosonization* procedure.

2.1 Walecka Model

This notes for this subsection are provided separately.

2.2 Nambu–Jona-Lasinio (NJL) Model

Here we will present an application of the HS technique to the NJL model for quark matter at finite densities and temperatures. This is possible since

the interaction of this model is of the current-current form and therefore the HS trick for the bosonization of 4-fermion interactions applies. The Lagrangian density is given by

$$\begin{aligned}
\mathcal{L} = & \bar{q}_{i\alpha}(i\cancel{\partial}\delta_{ij}\delta_{\alpha\beta} - M_{ij}^0\delta_{\alpha\beta} + \mu_{ij,\alpha\beta}\gamma^0)q_{j\beta} \\
& + G_S \sum_{a=0}^8 \left[(\bar{q}\tau_f^a q)^2 + (\bar{q}i\gamma_5\tau_f^a q)^2 \right] \\
& + G_D \sum_{k,\gamma} \left[(\bar{q}_{i\alpha}\epsilon_{ijk}\epsilon_{\alpha\beta\gamma}q_{j\beta}^C)(\bar{q}_{i'\alpha'}\epsilon_{i'j'k}\epsilon_{\alpha'\beta'\gamma}q_{j'\beta'}) \right. \\
& \left. + (\bar{q}_{i\alpha}i\gamma_5\epsilon_{ijk}\epsilon_{\alpha\beta\gamma}q_{j\beta}^C)(\bar{q}_{i'\alpha'}i\gamma_5\epsilon_{i'j'k}\epsilon_{\alpha'\beta'\gamma}q_{j'\beta'}) \right], \quad (89)
\end{aligned}$$

where from here on the quark spinor is $q_{i\alpha}$, with the flavor index $i = u, d, s$ and $\alpha = r, g, b$ stands for the color degree of freedom. $M_{ij}^0 = \text{diag}(m_u^0, m_d^0, m_s^0)$ is the current quark mass matrix in flavor space and $\mu_{ij,\alpha\beta}$ is the chemical potential matrix in color and flavor space. The grand cononical thermodynamical potential $\Omega = T \ln Z$ is known once we manage to evaluate the partition function in a reasonable approximation. A closed solution, even for the simple model Lagrangian (89), is not possible. The bosonization of the partition function proceeds as follows

$$\begin{aligned}
Z &= \int \mathcal{D}\bar{q}\mathcal{D}q \exp \int d^4x \mathcal{L} \\
&= \int \mathcal{D}\bar{q}\mathcal{D}q \prod_{i=u,d,s} \mathcal{D}\phi_i \prod_{k\gamma=ur,dg,sb} \mathcal{D}\Delta_{k\gamma} \mathcal{D}\Delta_{k\gamma}^\dagger \exp \int d^4x \mathcal{L}^{HS} \quad (90)
\end{aligned}$$

where the effective 'linearized' Lagrangian is given by

$$\begin{aligned}
\mathcal{L}^{HS} = & \bar{q}_{i\alpha} \left[i\cancel{\partial}\delta_{ij}\delta_{\alpha\beta} - (M_{ij}^0 - \phi_i\delta_{ij})\delta_{\alpha\beta} + \mu_{ij,\alpha\beta}\gamma^0 \right] q_{j\beta} \\
& - \sum_{i=u,d,s} \frac{\phi_i^2}{8G_S} - \sum_{k\gamma=ur,dg,sb} \frac{|\Delta_{k\gamma}|^2}{4G_D} + \bar{q}_{i\alpha} \frac{\Delta_{k\gamma}}{2} q_{j\beta}^C + \bar{q}_{i\alpha}^C \frac{\Delta_{k\gamma}^\dagger}{2} q_{j\beta} \quad (91)
\end{aligned}$$

The fermionic quark spinor fields can be grouped into bi-spinors, formed by the original and the charge-conjugated, transposed anti-spinor. This way, the action functional can be given the quadratic form which allows to integrate out the elementary quark fields using the Gaussian Functional Integration rule, thus leaving us after this exact Hubbard-Stratonovich transformation with an alternative representation of the partition function in terms of collective fields ϕ_i and $\Delta_{k\gamma}$.

The next step is the mean-field approximation, which consists of replacing the collective fields by those values which make the action functional extremal and neglecting the fluctuations around them, i.e. dropping the functional integration over these collective fields. This yields the thermodynamic potential

$$\begin{aligned}
\Omega(T, \mu) &= \frac{\phi_u^2 + \phi_d^2 + \phi_s^2}{8G_S} + \frac{|\Delta_{ud}|^2 + |\Delta_{us}|^2 + |\Delta_{ds}|^2}{4G_D} \\
&- T \sum_n \int \frac{d^3p}{(2\pi)^3} \frac{1}{2} \text{Tr} \ln \left(\frac{1}{T} S^{-1}(i\omega_n, \vec{p}) \right) \\
&+ \Omega_e - \Omega_0.
\end{aligned} \tag{92}$$

Here $S^{-1}(p)$ is the inverse propagator of the quark fields at four momentum $p = (i\omega_n, \vec{p})$,

$$S^{-1}(i\omega_n, \vec{p}) = \begin{bmatrix} \not{p} - M + \mu\gamma^0 & \Delta_{k\gamma} \\ \Delta_{k\gamma}^\dagger & \not{p} - M - \mu\gamma^0 \end{bmatrix}, \tag{93}$$

and $\omega_n = (2n + 1)\pi T$ are the Matsubara frequencies for fermions. The thermodynamic potential of ultrarelativistic electrons,

$$\Omega_e = -\frac{1}{12\pi^2} \mu_Q^4 - \frac{1}{6} \mu_Q^2 T^2 - \frac{7}{180} \pi^2 T^4, \tag{94}$$

has been added to the potential, and the vacuum contribution,

$$\begin{aligned}
\Omega_0 = \Omega(0, 0) &= \frac{\phi_{0u}^2 + \phi_{0d}^2 + \phi_{0s}^2}{8G_S} \\
&- 2N_c \sum_i \int \frac{d^3p}{(2\pi)^3} \sqrt{M_i^2 + p^2},
\end{aligned} \tag{95}$$

has been subtracted in order to get zero pressure in vacuum. Using the identity $\text{Tr}(\ln(D)) = \ln(\det(D))$ and evaluating the determinant (see Appendix A), we obtain

$$\ln \det \left(\frac{1}{T} S^{-1}(i\omega_n, \vec{p}) \right) = 2 \sum_{a=1}^{18} \ln \left(\frac{\omega_n^2 + \lambda_a(\vec{p})^2}{T^2} \right). \tag{96}$$

The quasiparticle dispersion relations, $\lambda_a(\vec{p})$, are the eigenvalues of the Hermitian matrix,

$$\mathcal{M} = \begin{bmatrix} -\gamma^0 \vec{\gamma} \cdot \vec{p} - \gamma^0 M + \mu & \gamma^0 \Delta_{k\gamma} C \\ \gamma^0 C \Delta_{k\gamma}^\dagger & -\gamma^0 \vec{\gamma}^T \cdot \vec{p} + \gamma^0 M - \mu \end{bmatrix}, \tag{97}$$

in color, flavor, and Nambu-Gorkov space. This result is in agreement with [?, ?]. Finally, the Matsubara sum can be evaluated on closed form [?],

$$T \sum_n \ln \left(\frac{\omega_n^2 + \lambda_a^2}{T^2} \right) = \lambda_a + 2T \ln(1 + e^{-\lambda_a/T}), \tag{98}$$

leading to an expression for the thermodynamic potential on the form

$$\begin{aligned}
\Omega(T, \mu) &= \frac{\phi_u^2 + \phi_d^2 + \phi_s^2}{8G_S} + \frac{|\Delta_{ud}|^2 + |\Delta_{us}|^2 + |\Delta_{ds}|^2}{4G_D} \\
&- \int \frac{d^3p}{(2\pi)^3} \sum_{a=1}^{18} \left(\lambda_a + 2T \ln \left(1 + e^{-\lambda_a/T} \right) \right) \\
&+ \Omega_e - \Omega_0.
\end{aligned} \tag{99}$$

It should be noted that (14) is an even function of λ_a , so the signs of the quasiparticle dispersion relations are arbitrary. In this paper, we assume that there are no trapped neutrinos. This approximation is valid for quark matter in neutron stars, after the short period of deleptonization is over.

Equations (94), (95), (97), and (99) form a consistent thermodynamic model of superconducting quark matter. The independent variables are μ and T . The gaps, ϕ_i , and Δ_{ij} , are variational order parameters that should be determined by minimization of the grand canonical thermodynamical potential, Ω . Also, quark matter should be locally color and electric charge neutral, so at the physical minima of the thermodynamic potential the corresponding number densities should be zero

$$n_Q = -\frac{\partial \Omega}{\partial \mu_Q} = 0, \tag{100}$$

$$n_8 = -\frac{\partial \Omega}{\partial \mu_3} = 0, \tag{101}$$

$$n_3 = -\frac{\partial \Omega}{\partial \mu_8} = 0. \tag{102}$$

The pressure, P , is related to the thermodynamic potential by $P = -\Omega$ at the global minima of Ω . The quark density, entropy and energy density are then obtained as derivatives of the thermodynamical potential with respect to μ , T and $1/T$, respectively.

The numerical solutions to be reported in this Section are obtained with the following set of model parameters, taken from Table 5.2 of Ref. [?] for vanishing 't Hooft interaction,

$$m_{u,d}^0 = 5.5 \text{ MeV} , \tag{103}$$

$$m_s^0 = 112.0 \text{ MeV} , \tag{104}$$

$$G_S \Lambda^2 = 2.319 , \tag{105}$$

$$\Lambda^2 = 602.3 \text{ MeV} . \tag{106}$$

With these parameters, the following low-energy QCD observables can be reproduced: $m_\pi = 135 \text{ MeV}$, $m_K = 497.7 \text{ MeV}$, $f_\pi = 92.4 \text{ MeV}$. The value of the diquark coupling strength $G_D = \eta G_S$ is considered as a free parameter of the model. Here we present results for $\eta = 0.75$ (intermediate coupling) and $\eta = 1.0$ (strong coupling).

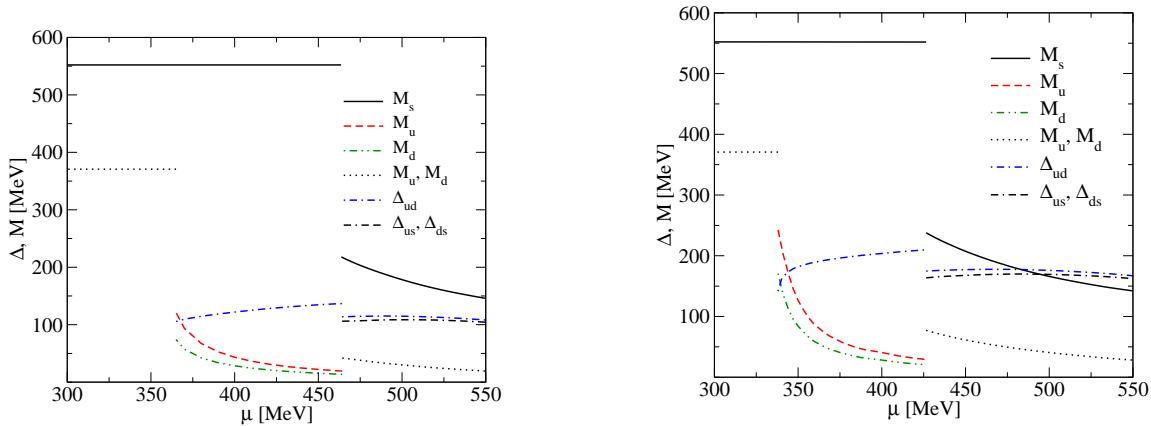


Figure 1: Gaps and dynamical quark masses as a function of μ at $T=0$ for intermediate diquark coupling, $\eta = 0.75$ (left) and for strong diquark coupling, $\eta = 1$ (right).

2.2.1 Quark masses and pairing gaps at zero temperature

The dynamically generated quark masses and the diquark pairing gaps are determined selfconsistently at the absolute minima of the thermodynamic potential, in the plane of temperature and quark chemical potential. This is done for both the strong and the intermediate diquark coupling strength. In Figs. 1 and 2 we show the dependence of masses and gaps on the quark chemical potential at $T = 0$ for $\eta = 0.75$ and $\eta = 1.0$, resp. A characteristic feature of this dynamical quark model is that the critical quark chemical potentials where light and strange quark masses jump from their constituent mass values down to almost their current mass values do not coincide. With increasing chemical potential the system undergoes a sequence of two transitions: (1) vacuum \rightarrow two-flavor quark matter, (2) two-flavor \rightarrow three-flavor quark matter. The intermediate two-flavor quark matter phase occurs within an interval of chemical potentials typical for compact star interiors. While at intermediate coupling the asymmetry between of up and down quark chemical potentials leads to a mixed NQ-2SC phase below temperatures of 20-30 MeV, at strong coupling the pure 2SC phase extends down to $T=0$. Simultaneously, the limiting chemical potentials of the two-flavor quark matter region are lowered by about 40 MeV. Three-flavor quark matter is always in the CFL phase where all quarks are paired. The robustness of the 2SC condensate under compact star constraints, with respect to changes of the coupling strength, as well as to a softening of the momentum cutoff by a formfactor, has been recently investigated within a different parametrization [?] with similar trend: for $\eta = 0.75$ and NJL formfactor the 2SC condensate does not occur for moderate chemical potentials while for $\eta = 1.0$ it occurs simultaneously with

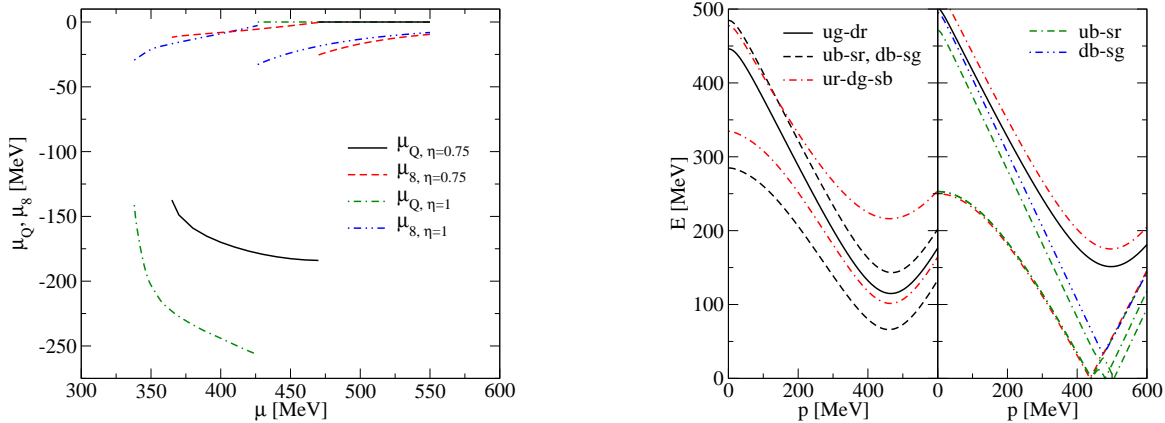


Figure 2: Left: Chemical potentials μ_Q and μ_8 at $T=0$ for both values of the diquark coupling $\eta = 0.75$ and $\eta = 1$. All phases considered in this work have zero n_3 color charge for $\mu_3 = 0$, hence μ_3 is omitted in the plot. Right: Quark-quark quasiparticle dispersion relations. For $\eta = 0.75$, $T = 0$, and $\mu = 480$ MeV (left panel) there is a forbidden energy band above the Fermi surface. All dispersion relations are gapped at this point in the $\mu - T$ plane, see Fig. 5. There is no forbidden energy band for the $ub - sr$, $db - sq$, and $ur - dg - sb$ quasiparticles at $\eta = 1$, $T = 84$ MeV, and $\mu = 500$ MeV (right panel). This point in the $\mu - T$ plane constitute a part of the gapless CFL phase.

chiral symmetry restoration. Fig. 3 shows the corresponding dependences of the chemical potentials conjugate to electric (μ_Q) and color (μ_8) charges. All phases considered in this work have zero n_3 color charge for $\mu_3 = 0$.

2.2.2 Dispersion relations and gapless phases

In Fig. 4 we show the quasiparticle dispersion relations of different excitations at two points in the phase diagram: (I) the CFL phase (left panel), where there is a finite energy gap for all dispersion relations. (II) the gCFL phase (right panel), where the energy spectrum is shifted due to the asymmetry in the chemical potentials, such that the CFL gap is zero and (gapless) excitations with zero energy are possible. In the present model, this phenomenon occurs only at rather high temperatures, where the condensates are diminished by thermal fluctuations.

2.2.3 Phase diagram

The thermodynamical state of the system is characterized by the values of the order parameters and their dependence on T and μ . Here we illustrate this dependency in a phase diagram. We identify the following phases:

1. NQ: $\Delta_{ud} = \Delta_{us} = \Delta_{ds} = 0$;

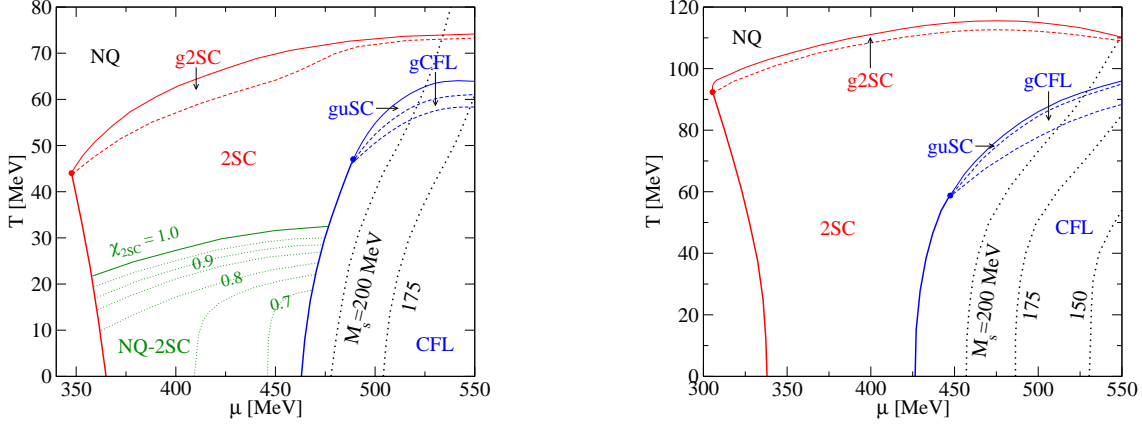


Figure 3: Left: Phase diagram of neutral three-flavor quark matter for intermediate diquark coupling $\eta = 0.75$. First-order phase transition boundaries are indicated by bold solid lines, while thin solid lines correspond to second-order phase boundaries. The dashed lines indicate gapless phase boundaries. The volume fraction, χ_{2SC} , of the 2SC component of the mixed NQ-2SC phase is denoted with thin dotted lines, while the constituent strange quark mass is denoted with bold dotted lines. Right: Phase diagram of neutral three-flavor quark matter for strong diquark coupling $\eta = 1$. Line styles as in previous Figures.

2. NQ-2SC: $\Delta_{ud} \neq 0$, $\Delta_{us} = \Delta_{ds} = 0$, $0 < \chi_{2SC} < 1$;
3. 2SC: $\Delta_{ud} \neq 0$, $\Delta_{us} = \Delta_{ds} = 0$;
4. uSC: $\Delta_{ud} \neq 0$, $\Delta_{us} \neq 0$, $\Delta_{ds} = 0$;
5. CFL: $\Delta_{ud} \neq 0$, $\Delta_{ds} \neq 0$, $\Delta_{us} \neq 0$;

and their gapless versions.

The resulting phase diagrams for intermediate and strong coupling are given in Figs. 5 and 6, resp. and constitute the main result of this work, which is summarized in the following statements:

1. Gapless phases occur only at high temperatures, above 50 MeV (intermediate coupling) or 60 MeV (strong coupling).
2. CFL phases occur only at rather high chemical potential, well above the chiral restoration transition, i.e. above 464 MeV (intermediate coupling) or 426 MeV (strong coupling).
3. Two-flavor quark matter for intermediate coupling is at low temperatures ($T < 20$ -30 MeV) in a mixed NQ-2SC phase, at high temperatures in the pure 2SC phase.
4. Two-flavor quark matter for strong coupling is in the 2SC phase with rather high critical temperatures of ~ 100 MeV.

5. The critical endpoint of first order chiral phase transitions is at $(T, \mu) = (44 \text{ MeV}, 347 \text{ MeV})$ for intermediate coupling and at $(92 \text{ MeV}, 305 \text{ MeV})$ for strong coupling.

2.3 Mesonic correlations at finite temperature

In the previous section we have seen how the concept of order parameters can be introduced in quantum field theory in the mean-field approximation. By analysis of the gap equations describing the minima of the thermodynamical potential in the space of order parameters we have we could investigate the phenomenon of spontaneous symmetry breaking, indicated by a nonvanishing value of the order parameter (gap). Important examples being: chiral symmetry breaking (mass gap) and superconductivity (energy gap). At finite temperature and density the values of these gaps change and their vanishing indicates the restoration of a symmetry. As the symmetries prevailing under given thermodynamical conditions of temperature and chemical potential (density) characterize a phase of the system, we have thus acquainted ourselves with a powerful quantum field theoretical method of analysing phase transitions. The results of such an analysis are summarized in phase diagrams. A prominent example is the phase diagram of QCD in the temperature- density plane, shown schematically in Fig. ???. It exhibits two major domains: Hadronic matter (confined quarks and gluons) and the Quark-gluon plasma (QGP), separated by the phenomenon of quark (and gluon) deconfinement under investigation in heavy-ion collisions, but also in the physics of compact stars and in simulations of Lattice-gauge QCD on modern Teraflop computers. The hadronic phase is subdivided into a nuclear matter phase at low temperatures with a gas-liquid transition (similar to the van-der-Waals treatment of real gases) and a 'plasma phase' of a hot hadron gas with a multitude of hadronic resonances. The QGP phase is subdivided into a quark matter phase at low temperatures where most likely gluons are still condensed (confined) and the strongly correlated Fermi-liquid of quarks should exhibit the phenomenon of superconductivity/ superfluidity with a Bose condensate of Cooper pairs of . diquarks. At asymptotic temperatures and densities one expects a system of free quarks and gluons (due to asymptotic freedom of QCD). In any real situation in terrestrial experiments or in astrophysics, one expects to be quite far from this ideal gas state. As the nature of the confinement-deconfinement transition is not yet clarified, we must speculate what to expect in the vicinity of the conjectured deconfinement phase transition. In the lattice-QCD simulations one has found evidence for strong correlations even above the critical temperature $T_c \sim 170$ MeV, which is defined by an increase of the effective number of degrees of freedom $\varepsilon(T)/T^4$ by about one order of magnitude in a close vicinity of T_c . Indications for strong correlations in the QGP one has also found in recent RHIC experiments, where from particle production and flow one has found fast thermalization and an extremely low viscosity ('perfect fluid'). One speaks about an 'sQGP phase' at temperatures $T_c \lesssim T \lesssim 2 T_c$.

In order to investigate the phase diagram experimentally, one has to correlate the observables with the regions. As the detectors are situated in the 'vacuum' at zero temperature and chemical potential where confine-

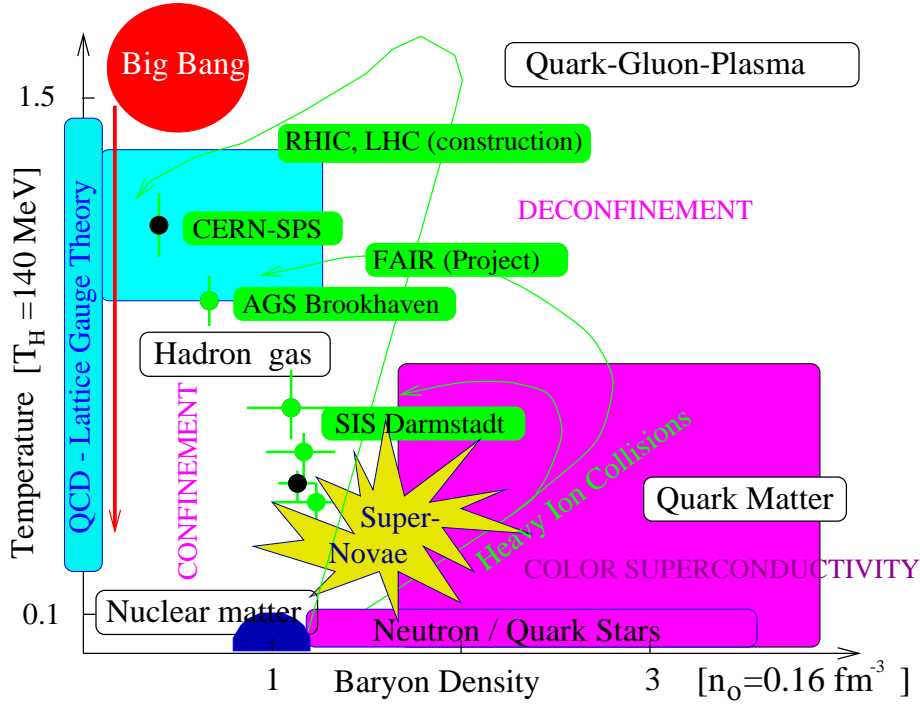


Figure 4: The conjectured phase diagram of QCD and places where to investigate it.

ment prevails, no direct detection of quarks and gluons from the plasma phase is possible and one has to conjecture about the properties of the sQGP phase(s) from the traces which they might leave in the hadronic and electromagnetic spectra emitted by the hadronizing fireball formed in a heavy-ion collision or by the neutrino-emitting cooling processes of compact stars.

As a prerequisite for discussing hadronic spectra and their modifications, we will study the mesonic spectral function(s), and for their analysis within effective models like the NJL or MN models, we need to evaluate loop diagrams at finite temperature. A basic ingredient are Matsubara frequency sums.

2.4 Matsubara frequency sums

In computing Feynman diagrams with internal fermion lines we shall encounter frequency sums, and we have to learn how to evaluate them. Let us denote the quantity $(\omega_n^2 + E_p^2)^{-1}$, which appears in the free Fermion propagator

$$S_F(i\omega_n, \mathbf{p}) = - \int_{-\infty}^{\infty} \frac{d\mathbf{p}_0}{2\pi} \frac{\rho_F(\mathbf{p}_0, \mathbf{p})}{i\omega_n - \mathbf{p}_0} = \frac{\mathbf{m} - \not{\mathbf{p}}}{\omega_n^2 - \mathbf{E}_p^2} \quad (107)$$

by $\tilde{\Delta}(i\omega_n, E_p)$, and its mixed representation by $\tilde{\Delta}(\tau, E_p)$, suppressing the subscript F for simplicity

$$\tilde{\Delta}(\tau, E_p) = T \sum_n e^{-i\omega_n \tau} \tilde{\Delta}(i\omega_n, E_p) . \quad (108)$$

It can easily be checked (**Exercise !**) that

$$\begin{aligned} \tilde{\Delta}(\tau, E_p) &= \frac{1}{2E_p} \left[(1 - \tilde{n}(E_p)) e^{-E_p \tau} - \tilde{n}(E_p) e^{E_p \tau} \right] \\ &= \sum_{s=\pm 1} \frac{s}{2E_p} (1 - \tilde{f}(sE_p)) e^{-sE_p \tau} , \end{aligned} \quad (109)$$

where the Fermi-Dirac distribution $\tilde{n}(p_0)$ is

$$\tilde{n}(p_0) = \frac{1}{e^{\beta|p_0|} + 1} . \quad (110)$$

One should note the absolute value of p_0 in (110), in contrast with the definition of $\tilde{f}(p_0) = 1/[\exp(\beta p_0) + 1]$. Note also that

$$\begin{aligned} \tilde{f}(E) &= \tilde{n}(E) , \quad \tilde{f}(-E) = 1 - \tilde{n}(E) , \\ 1 - \tilde{f}(E) - \tilde{f}(-E) &= 0 . \end{aligned} \quad (111)$$

In frequency space, the formula corresponding to (109) is

$$\begin{aligned} \tilde{\Delta}(i\omega_n, E_p) &= \frac{1}{\omega_n^2 - E_p^2} = \sum_{s=\pm 1} \tilde{\Delta}_s(i\omega_n, E_p) \\ &= \sum_{s=\pm 1} -\frac{s}{2E_p} \frac{1}{i\omega_n - sE_p} . \end{aligned} \quad (112)$$

The frequency sums are performed by following the methods of analytic continuation $i\omega_n \rightarrow k_0$ and contour integration with a function having simple poles at the discrete frequencies $k_0 = i\omega_n$ with unit residuum and convergence for $|k_0| \rightarrow \infty$. Let us give two general examples for Matsubara sums of one-loop diagrams with two external (amputated) legs.

- Fermion-boson case, see Fig. 2.4:

$$T \sum_n \Delta_{s_1}(i\omega_n, E_1) \tilde{\Delta}_{s_2}(i(\omega - \omega_n), E_2) = -\frac{s_1 s_2}{4E_1 E_2} \frac{1 + f(s_1 E_1) - \tilde{f}(s_2 E_2)}{i\omega - s_1 E_1 - s_2 E_2} \quad (113)$$

$$T \sum_n \omega_n \Delta_{s_1}(i\omega_n, E_1) \tilde{\Delta}_{s_2}(i(\omega - \omega_n), E_2) = -\frac{i s_2}{4E_2} \frac{1 + f(s_1 E_1) - \tilde{f}(s_2 E_2)}{i\omega - s_1 E_1 - s_2 E_2} \quad (114)$$

- Fermion-antifermion case, see Fig. 2.4:

$$T \sum_n \tilde{\Delta}_{s_1}(i\omega_n, E_1) \tilde{\Delta}_{s_2}(i(\omega - \omega_n), E_2) = -\frac{s_1 s_2}{4E_1 E_2} \frac{1 - \tilde{f}(s_1 E_1) - \tilde{f}(s_2 E_2)}{i\omega - s_1 E_1 - s_2 E_2} \quad (115)$$

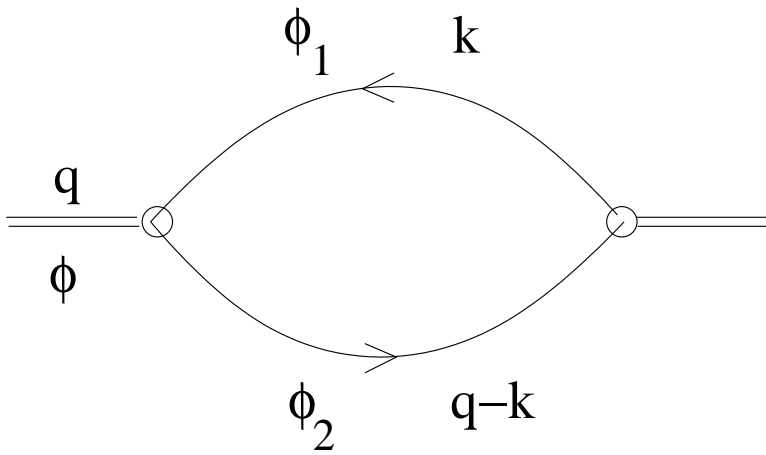


Figure 5: One-loop diagram for the fermion-antifermion polarization function.

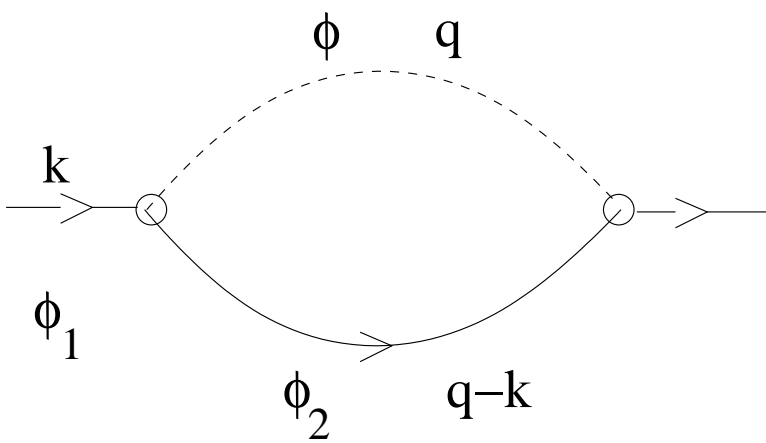


Figure 6: One-loop diagram for the fermion self-energy.

$$T \sum_n \omega_n \tilde{\Delta}_{s_1}(i\omega_n, E_1) \tilde{\Delta}_{s_2}(i(\omega - \omega_n), E_2) = -\frac{is_2}{4E_2} \frac{1 - \tilde{f}(s_1 E_1) - \tilde{f}(s_2 E_2)}{i\omega - s_1 E_1 - s_2 E_2} \quad (116)$$

Note that you can obtain unify these formula using the rule: $f(sE) \rightarrow -\tilde{f}(sE)$ when replacing a bosonic by a fermionic line.

Exercise: Verify these expressions!

References

- [1] J.I. Kapusta, Finite-temperature Field Theory, Cambridge University Press, 1989
- [2] M. Le Bellac, Thermal Field Theory, Cambridge University Press, 1996
- [3] D. Blaschke, et al., Phys. Rev. **D 72** (2005) 065020.